Integrated opto-microfluidics platforms in lithium niobate crystals for sensing applications

G. Bettella, G. Pozza, A. Zaltron, M.V Ciampolillo, N. Argiolas, C.Sada*
Physics and Astronomy Department "G.Galilei", University of Padova, Via MArzolo 8 35131 Padova (Italy)

M. Chauvet, B. Guichardaz
FEMTO-ST institute, UMR CNRS 6174, University of Franche-Comté, 15B Avenue des Montboucons, 25000 Besançon (France)

*Corresponding author: C. Sada, cinzia.sada@unipd.it

Keywords:
Optofluidics, micro-fluidics, optical waveguides, integrated optics, lithium niobate

ABSTRACT

In micro-analytical chemistry and biology applications, droplet microfluidic technology holds great promise for efficient lab-on-chip systems where higher levels of integration of different stages on the same platform is constantly addressed. The possibility of integration of opto-microfluidic functionalities in lithium niobate ($LiNbO_3$) crystals is presented. Microfluidic channels were directly engraved in a $LiNbO_3$ substrate by precision saw cutting, and illuminated by optical waveguides integrated on the same substrate. The morphological characterization of the microfluidic channel and the optical response of the coupled optical waveguide were tested. In particular, the results indicate that the optical properties of the constituents dispersed in the fluid flowing in the microfluidic channel can be monitored in situ, opening to new compact optical sensor prototypes based on droplets generation and optical analysis of the relative constituents.

1. INTRODUCTION

Microfluidic technology holds great promise as it can perform typical laboratory applications using a fraction of the volume of reagents in significantly less time. Reagents can be significantly reduced from millilitres and microliters to nanolitres and femtolitres whereas hours of reaction time could be decreased to mere seconds or less [1]. Applications for microfluidics have significantly advanced from its root in micro-analytical chemistry to include high throughput screening, biological analysis of cells and proteins and reaction kinetics and mechanism studies. [2]. Due to the high surface area to volume ratios, the reaction times are faster and the independent control of each droplet can be exploited to realise micro-reactors that can be individually transported, mixed and analysed. Thanks to its scalability and parallel processing, the droplets microfluidics has been used in a wide range of applications including the synthesis of biomolecules, drug delivery and diagnostic testing and bio-sensing [3; 4]. Although novel micro-fabrication techniques are continuously being developed and micro-chemical systems are established by integrating micro-devices with appropriate fluidic interfacing scheme, the incorporation of chemical and physical

sensors perfectly integrated with the micro-reactor stage is still under debate although the optical VIS-NIR methods are the most used to get quantification and chemical identification. The most commonly used materials for micro-reactors based device (such as ceramics, polymers, stainless steel, glasses, silica and silicon) in fact, seem to prevent the fully integration the microfluidic and optical functionalities in the VIS-NIR region although presenting bio- and micro-machining compatibility. As a matter of fact several examples of sensors for reaction temperature, residence time and stoichiometry have been reported [5] as well as systems for in-situ reaction monitoring with fluorescent measurements, with line ultraviolet spectroscopy, with inline infrared and Raman spectroscopy [2; 6]. In this scenario, the integration of a large number of different stages on a single substrate chip is a key point for promoting new insights in many applications that need portable devices to speed the analysis and allow investigation of new phenomena [7, 8]. Among the others, even lithium niobate ($LiNbO_3$) crystals have been proposed in microfluidics since allows for high efficient acoustic waves generation to move droplets on the substrate in a very controlled way [9], flow mixing and pumping [10], pyroelectric [11] and photogalvanic particle trapping[12]. Quite surprisingly, all the above mentioned applications were realized without producing a microfluidic circuit directly on $LiNbO_3$ substrates and without the integration of optical sensing stages although it is a material thoroughly exploited in the photonic and integrated optics industry. As a matter of fact waveguides and a large number of integrated electro-optical devices such as switches, modulators and directional couplers are still commercial in $LiNbO_3$. Diffractive optical elements such as holographic filters and multi/demultiplexers were in fact proposed by exploiting its photorefractive effect strongly enhanced by local doping with metal impurities, [13]. Furthermore, its remarkable optical coefficients and significant photorefractive response have allowed to exploit this material for the realization of various optical systems, such as second-harmonic generation, optical modulator and waveguides, particles and droplet manipulation and so on [14-18].

Moreover, the recent development of techniques able to modify this material at a micro- and nanometer scale has led to a progressive increasing interest in it by the side of both the scientific and the industrial communities, thus promoting theoretical and experimental studies on pure and doped $LiNbO_3$ crystals.

Recently lithium niobate has been also proposed as candidate for application in opto-microfluidic technology [19, 20,21], thus combining the tools typical of microfluidics with the potentialities offered by this material. A further improvement could come from the integration on the same substrate of different functionalities such as a T-shaped droplet generator and optical stages to obtain a system able to perform on-site optical sensing processes such as those required in chemical and biological analyses. In this case, therefore, starting from the droplet generation and manipulation, consider the droplets transfer through a microfluidic channel directly engraved on the crystal substrate to an integrated analysis stage where the optical properties of the droplets constituents are monitored and detected. The realization of such a device prototype requires different preparation steps, from the creation of the microfluidic droplet generation and the implementation of channel waveguides for the optical sensing of the droplets.

In this work, by a step-by-step logic, we will describe the recent results on the realisation of each of the mentioned stages focusing on the fabrication of micro-fluidic channel coupled with optical waveguide integrated on the same substrate on X-cut lithium niobate crystals. The relative characterization of each stage is presented to qualify the relative performances with the aim of addressing the potential realization of optical sensing platforms. In particular, the microfluidic stage was realized by using the precision sawing method instead of laser ablation as reported in [22]. The optical waveguides coupled to the microfluidic channels were integrated on the same substrate by exploiting Ti in-diffusion process on photolithographically pattern channel instead of exploiting photorefractive beam self-trapping process controlled by the pyroelectric effect respectively as proposed in [20]. This approach aims to investigate the feasibility of getting opto-fluidic circuit by standard techniques already available at an industry level.

2. EXPERIMENTAL

2.1 Microfluidic Stage

Microfluidics-channels were cut with a precision saw (Disco DAD 321) in order to assure a high optical grade dicing. From a commercial lithium niobate wafer (Crystal Technology) with congruent composition several x-cut samples of about 2x2 cm^2 were cut and then mantained on the holder by a UV sensitive adhesive film. Since polished faces are requested at both the entrance and exit side as well as at the walls of the trenches, in order to limit losses due to light diffusion, a polymer blade with diamond particles was used. Cutting parameters have been experimentally determined to give optical quality cuts in $LiNbO_3$. Typically, the blade, with a diameter of 56 mm and a thickness of 200μm, rotates at 10 Krpm and the cutting speeds was fixed at 0.2 mm s^{-1}, respectively. A constant and high flow of water was exploited, keeping a constant and low temperature for both the blade and the sample during the process. Such a process constitutes a straightforward way to simultaneously dice and polish 200μm wide by 50μm deep trenches oriented along the z-axis, with smooth walls and realized in a single step process. Note that trenches can have open or closed ends by controlling the blade trajectory.
The surface quality of the engraved microfluidic channels was performed by monitoring the morphology of the walls and of the bottom of the cut. Atomic Force Microscopy was consequently used together with standard profilometer techniques in order to quantify both the roughness and the geometrical characteristics of the micro-channels. A (KLA Tencor P-10) was exploited with a typical resolution The profilometer was also exploited to estimate the roughness R_a relative to the bottom of each microfluidic channel, thus comparing the obtained value with those relative to other techniques.
The microfluidic channel was filled by Hexadecane (CAS number: 544-76-3, viscosity 3cP, density 0.77 g/cm^3). $LiNbO_3$ was completely wetted by the hexadecane (Contact Angle<10°) but demonstrated to be moderately hydrophobic (Contact Angle close to 60°).

2.2 Optical waveguide Stage

The micro-fluidic stage was coupled to the optical waveguides to the microfluidic channel to get the final device prototype as sketched in Fig.1. The input optical waveguide plays the role of illuminating the microfluidic channel filled by fluid and therefore is referred as pump waveguide. The light transmitted through the microfluidic channel can be gathered by the output waveguide and therefore recorded. Both waveguides were realized by exploiting the standard Titanium in-diffusion process combined with suitable photolithographic patterning in order to realize 2D channel waveguide. In particular Ti strips with a width of (5.9 ± 0.2) μm were deposited by means of the RF sputtering process (deposition rate (47 ± 2) x 10^{15} at/cm^2 s) on masked open channels realised by standard photolithographic techniques [23]. Taking into account the diffusion coefficient of Ti inside our lithium niobate substrate ((88 ± 8) nm^2/s), the in-diffusion of the channel strips was performed by annealing the samples in controlled O_2 atmosphere (50Nl/h) at 1030°C for 2h in order to get channel optical waveguide supporting one optical mode. The in-depth profile of the waveguides was obtained by exploiting the Secondary Ion Mass Spectrometry technique. As expected from Fick's law the Ti concentration inside the substrate follows a semi-gaussian profile, with a maximum dopant concentration at the surface of 5% mol and a FWHM of (1.29 ± 0.05) μm.
After polishing both the lateral faces of each sample, the Ti-diffused:$LiNbO_3$ optical waveguide were characterized by means of Near Field method. In this technique a microscope objective is positioned at the exit face of the waveguide in order to enlarge the beam spot before entering in the camera system. This allowed estimeting the performance of the channel waveguides before and after the realization of the crossing microfluidic channel. The optical characterization was performed by using a fiber-coupled diode laser at 670 nm, whose single mode beam was injected into the Ti:LN waveguides by exploiting a spherical lens (f = 20mm) and a microscope objective (magnification 20x, NA = 0.4). At the output of the optical waveguide the near-field image was collected by a Vidicon tube by using a 20x (f=10mm) objective lens and recorded by a digital camera (LaserCam-HR, Coeherent), which allows to verify as the presence of the microfluidic channel affect the intensity distribution of the guided beam.

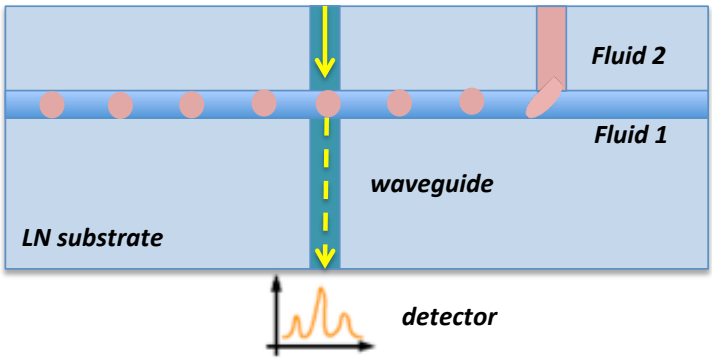

Fig.1 Sketch of the opto-fluidics device prototype for optical analysis of droplet.

3. RESULTS

Each stage of the opto-microfluidic device prototype was characterized in order to test the relative performances and finally optimise the relative integration efficiency.

3.1 Microfluidic stage: characterization.

The microfluidic channels were characterized by a morphological point of view by performing Atomic Force Microscopy and the geometrical size were measured by a Standard Tencor profilometer. As a matter of fact the roughness of the lateral and the bottom surfaces of the microfluidic channel strongly affect the performances of the final device, both concerning the transmitted intensity of the crossing waveguide and the fluidic movements of liquids and droplet inside the channel. The profilometer was used to measure the thickness and width of the engraved channels, which are 43.1 ± 0.1 μm and 204 ± 1 μm respectively.

In Fig. 2 we report the AFM images relative to both the bottom (a) and the lateral walls (b) of the microfluidic channel. The morphologic characterization showed that no periodic structures are present. In particular the average roughness at the bottom, which affect the fluidic performances of the channel, was found to be R_a = (18.8 ± 8.5) nm, that compared to the value obtained by the laser ablation technique (R_a = (260 ± 20) nm) reported in [articolo de Gruyter] is surely competitive, and strongly better than that observed in microfluidics channels engraved in lithium niobate by other precision blade for optical grade dicing (where R_a = (530 ± 10) nm was measured). Concerning the roughness of the lateral walls, it was estimated to be R_a = (6.8 ± 1.1) nm, that is smaller than the value measured on the bottom of the channel. The polymer blade with diamond particles used in this work, in fact, guarantees a good optical grade of the surfaces of the engraved channels, thus decreasing the total loss of the intensity beam when it crosses the microfluidic channel.

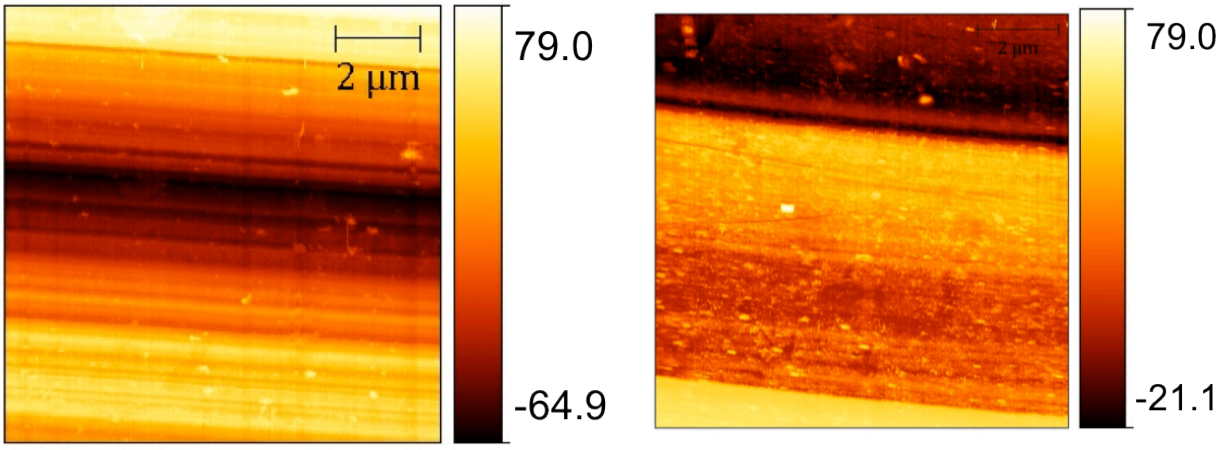

(a) (b)

Fig. 2 (a) AFM image of a 10 x10 μm^2 region of the bottom (a) and the lateral walls (b) of the microfluidic channel. The unit of the color scale is in nanometers.

3.1 Optical stage: waveguide characterization

The refractive index profile of an optical channel waveguide can be determined by means of different numerical approximations, such as the method of finite differences or finite elements, which can be used to calculate the effective refractive indices of the various modes guided by an assumed refractive index profile. However, these calculations are out of the scope of this work, so a maximum refractive index change at the surface of our waveguides has been estimated by using the relation proposed by E. Strake et al. [24]. As a matter of fact the method proposed by Strake allows directly deriving the refractive index profile by knowing the in-depth Ti concentration profile inside the lithium niobate substrate. In particular in our case we obtained a refractive index change at the surface of the doped area which is equal to $\Delta n_e = (1.12 \pm 0.03) \times 10^{-2}$ and $\Delta n_o = (0.66 \pm 0.02) \times 10^{-2}$.

Near-field measurements were carried out by connecting the digital camera to the computer and by controlling the intensity of the exiting beam after the fiber by using a diode laser driver. In particular, in our experiment the intensity of the beam was set to 2.2 x 10^5 W/m^2, which is the maximum value usable without damaging the video camera without the use of a neutral density. Moreover, at the entrance of the waveguide the waist of the beam was measured to be (5,30372 ± 1,1124) mm. The intensity distribution of the waveguided light was recorded before and after the creation of the transversal microfluidic channel, as well as in the center of the channel. In Fig.3 it is possible to observe the CCD image of the Light intensity spatial distribution of the TEM_{00} mode both in the sample without the microfluidic channel at the output face of the waveguide (a), and in the sample where the microfluidic channel is present (b). In particular the image reported in Fig.3 (b) is relative to the beam at the output wall of the microfluidic channel, that is when the beam has crossed the channel and enters in the second part of the waveguide. In this case the channel was not filled with liquids, so the beam travels in air when crossing the microfludicic channel. In Fig.3 (a) the beam present a well-defined shape, which is asymmetric in the vertical direction due to the fact that the Ti concentration in the doped area varies with depth, thus creating a gradient of the refractive index change. Moreover, it is possible to observe that the beam in (b) is larger than the one showed in (a), due to the divergence and diffraction of the guided beam that exits from the waveguide. As a consequence, even assuming that the two waveguides at the two sides of the microfluidic channel are perfectly aligned, after 200 μm, i.e. the

microfluidic channel width, only a portion of the incident beam can be coupled in the output waveguide and consequently the light intensity recorded at the end of the output waveguide is less than that exiting from the input waveguide and injected within the micro-fluidic channel. Fresnel reflections at the two air-LiNbO3 interfaces also contribute to the loss in transmission. This is the worst case, since the refractive index mismatch is higher when air permeates the fluidic channel. For this reason tests were also performed in the case of microfluidic channels filled with fluid. In particular the hexadecane was chosen as test fluid, since it is known to be hydrophilic and it presents a higher refractive index (n=1.43) than air at the working wavelength. In Fig. 4 the CCD image of the light intensity at the end of the second (output) waveguide is reported when air (Fig.4 a) and hexadecane (Fig.4 b) were injected in the microfluidic channel, respectively, and both the exiting beams show a well-defined shape. Moreover, it is possible to notice as in presence of the microfluidic channel the whole output intensity distribution presents a ring of light with lower intensity around the guided beam inside the sample (that is in the lower part of both the images reported in Fig.4). This light is mainly due to the portion of beam that is not coupled inside the output waveguide and that therefore distributes around the guided mode while travelling through the sample.

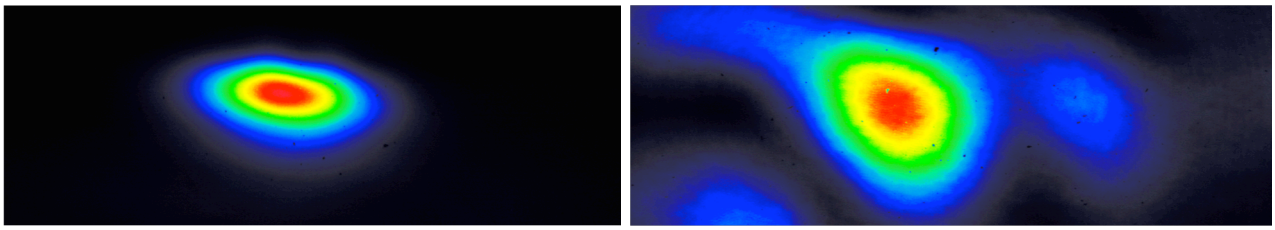

(a) (b)

Fig.3 Light intensity spatial distribution of the TEM_{00} mode: (a) in absence of the microfluidic channel, at the output face of the waveguide; (b) in presence of the microfluidic channel filled with air, at the entrance of the of the second part of the waveguide, that is after the microfluidic channel in air. The beam intensity at the entrance of the waveguide was 2.2 $x10^5$ W/m^2 and 4.8 $x10^5$ W/m^2.

As it is possible to notice, when the microfluidic channel is filled with hexadecane the intensity of the beam exiting from the final waveguides is significantly improved. As a matter of fact, when air permeates the channel the output beam presents a final intensity which is about 62% lower than the value measured in absence of the channel (Fig.3 (a)), whereas the intensity loss observed when the channel is filled with hexadecane is about 24%. Two effects contribute to improve the transmission. First, the refractive index of the hexadecane is closer to that of lithium niobate (n≈2.2) than air, thus reducing the intensity losses due to the Fresnel reflection of the beam at the interfaces with the microfluidic channel. Second, light diffraction is weaker in the channel filled with a high refractive index material, thus promoting a better coupling in the second waveguide.

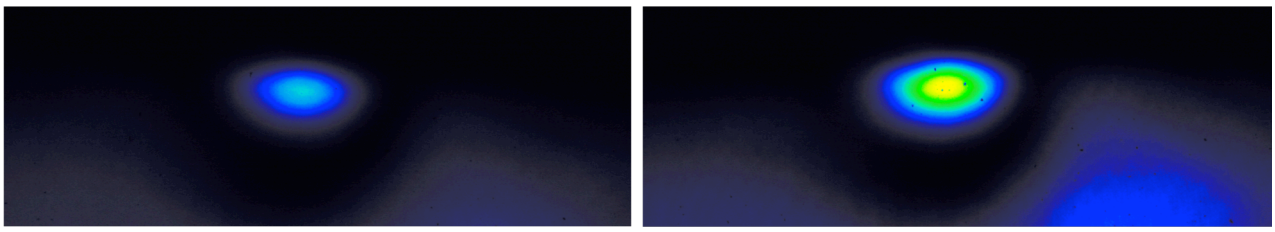

(a) (b)

Fig.4 Light intensity spatial distribution of the TEM_{00} mode: (a) at the end of the waveguide with a microfluidic channel filled with air; (b) at the end of the waveguide with the microfluidic channel filled with hexadecane. The intensity of the beam at the entrance of the waveguide was the same for both cases, that is 2.2 x 10^5 W/m^2.

4. CONCLUSIONS

Micro-fluidic channels realized by means of precision sawing in a lithium niobate crystal were optically coupled with channel waveguides integrated on the same substrate by means of Ti-indiffusion process, combined with suitable photolitoghaphic patterning. The relative characterization of each stage demonstrated that an opto-fluidics stage can be successfully realized in this material and that by implementing a T-junction configuration, even droplets could be efficiently illuminated and optically investigated. These results address the potential realization of optical sensing platforms, where the constituent of the droplet or article dissolved in liquids could be monitored. Finally, when high intensity coupling is needed and multimode propagation is required, waveguides realized by Ti-indiffusion could be considered as a valid alternative to those obtained by photorefractive beam self-trapping process controlled by the pyroelectric effect, as proposed in [17].

ACKNOWLEDGMENTS

The authors kindly acknowledge the Ca.Ri.Pa.Ro foundation for financing the research by the Excellence Project "Integrated opto-microfluidic prototype on lithium niobate crystals for sensing applications" (call 2011-2012) and the COST action MP1205 "Advances in Optofluidics: Integration of Optical Control and Photonics with Microfluidics". This work was partly supported by the RENATECH network and its FEMTO-ST technological facility.

REFERENCES

[1] The S.Y., Lin R., Hung L.Y. and Lee A.P., "Droplet microfluidics", Lab Chip 8, 198–220 (2008)
[2] McMullen J.P. and Jensen K.F., "Integrated microreactors for reaction automation: New approaches to reaction development", Annu. Rev. Anal. Chem. 3, 19-42 (2010);
[3] Watts P. and Haswell S.J., "The application of micro reactors for organic synthesis", Chem. Soc. Rev. 34, 235-246 (2005);
[4] Doku G. N., Verboom W., Reinhoudt D.N. and Van den Berg A., "On-microchip multiphase chemistry—a review of microreactor design principles and reagent contacting modes", Tetrahedron 61, 2733-2742 (2005);
[5] Quiram D.J., Jensen K.F., Schmidt M.A., Mills P. L., Ryley J. F., Wetzel M. D. and Kraus D. J., "Integrated Microreactor System for Gas-Phase Catalytic Reactions. 2. Microreactor Packaging and Testing", Ind. Eng. Chem. Res. 46, 8306-8316 (2007);
[6] Novak L., Neuzil P., Pipper J., Zhang Y. and Lee S., "An integrated fluorescence detection system for lab-on-a-chip applications", Lab chip 7, 27-29 (2007);
[7] Psaltis D., Quake S. R. and Yang C., "Developing optofluidic technology through the fusion of microfluidics and optics", Nature 442, (2006);
[8] Sin M., Gao J, Liao JC and Wong P., "System Integration – A major step toward lab on a chip", Jour. Biol. Eng. 5, 1-21 (2011);
[9] Friend J.R. and Yeo L.Y., "Microscale Acoustofluidics: Microfluidics Driven via Acoustics and Ultrasonics", Rev. of modern Physics 83, 647-704 (2011);
[10] Tan M. K., Yeo L. Y. and Friend J. R., "Rapid fluid flow and mixing induced in microchannels using surface acoustic waves", EPL 87, 47003 (2009);
[11] Grilli S. and Ferraro P., "Dielectrophoretic trapping of suspended particles by selective pyroelectric effect in lithium niobate crystals", Appl. Phys. Lett. 92, 232902 (2008);

[12] Esseling M., Holtmann F., Woerdermann M. and Denz C., “Two-dimensional dielectrophoretic particle trapping in a hybrid crystal/PDMS-system, ”Optic Express 18 (16), 17404 (2010);
[13] Volk, T. and Wöhlecke, M., *Lithium niobate: defects, photorefraction and ferroelectric switching*, Springer Series in Material Science, Berlin (2008);
[14] Denz C., Müller K.-O., Heimann T., and Tschudi T., “Volume holographic storage demonstrator based on phase-codedmultiplexing”, IEEE Journal of Selected Topics in Quantum Electronics 4, 832 (1998);
[15] Breer S. and Buse K., “Wavelength demultiplexing with volume phase holograms in photorefractive lithium niobate”, Applied Physics B 66, 339 (1998);
[16] Lee Y. L., Yu N. E., Jung C., Yu B.-A., Sohn I.-B., Choi S.-C., Noh Y.-C., Ko D.-K., Yang W.-S., Lee H.-M., Kim W.-K. and Lee H.-Y., “Second-harmonic generation in periodically poled lithiumniobate waveguides fabricated by femtosecond laser pulses”, Applied Physics Letters 89, 171103 (2006);
[17] Carrascosa M., Cabrera M. and Agulló-López F., “Long-Lifetime Photorefractive Holographic Devices via Thermal Fixing Methods”, Infrar. Holog. for Opt. Comm. 86, 91 (2003);
[18] Esseling, M., Zaltron, A., Sada, C., Denz, C. “Charge sensor and particle trap based on z-cut lithium niobate”, Appl. Phys. Lett. 103, 061115-1-3 (2013);
[19] Sridhar, M., Maurya, D.K., Friend, J.R., Yeo, L.Y., “Focused ion beam milling of microchannels in lithium niobate”, Biomicrofluidics 6 (1), 12819-128911 (2012);
[20] Chauvet, M., Al Fares, L., Devaux, F., “Self-trapped beams for fabrication of optofluidic chips” Proceeding SPIE vol. 8434 84340Q-2 (2012);
[21] M. Esseling, A. Zaltron, W. Horn and C. Denz, “Optofluidic droplet router”, Laser & Photonics Rev. 9, 98, 2015;
[22] Pozza, G., Kroesen, S. , Bettella, G., Zaltron, A., Esseling, M., Mistura, G., Sartori, P., Chiarello, E., Pierno, M., Denz, C., Sada, C., “T-junction droplet generator realised in lithium niobate crystals by laser ablation”, Optofluid. Microfluid. Nanofluid. 1, 34, 2014;
[23] Hu H., Ricken R. and Sohler W., “Low-loss ridge waveguides on lithium niobate fabricated by local diffusion doping with titanium”, Appl Phys B 98, 677–679, (2010),
[24] Strake E., Bava G.P. and Motrosset I., “Guided modes of Ti.$LiNbO_3$ channel waveguides: a novel quasi-analytical technique in comparison with the scalar finite-element method”, J. Lightwave Tech. 6 (6), 1126 (1998);